A STOCHASTIC MODEL OF THE MELANOPSIN PHOTOTRANSDUCTION CASCADE

R. LANE BROWN*, ERIKA CAMACHO†, EVAN G. CAMERON ‡, CHRISTINA HAMLET §, KATHLEEN A. HOFFMAN ¶, HYE-WON KANG ‖, PHYLLIS R. ROBINSON **, KATHERINE S. WILLIAMS ††, AND GLENN R. WYRICK ‡‡

Abstract.
Melanopsin is an unusual vertebrate photopigment that, in mammals, is expressed in a small subset of intrinsically photosensitive retinal ganglion cells (ipRGCs), whose signaling has been implicated in non-image forming vision, regulating such functions as circadian rhythms, pupillary light reflex, and sleep. The biochemical cascade underlying the light response in ipRGCs has not yet been fully elucidated. We developed a stochastic model of the hypothesized melanopsin phototranduction cascade and illustrate that the stochastic model can qualitatively reproduce experimental results under several different conditions. The model allows us to probe various mechanisms in the phototransduction cascade in a way that is not currently experimentally feasible.

Key words. melanopsin, law of mass action, phototransduction cascade, Markov-chain model, Gillespie's algorithm

AMS(MOS) subject classifications. 92C45 (Kinetics in Biochemical Problems), 80A30 (Chemical Kinetics)

1. Introduction.

The mammalian retina, located at the back of the eye, is the only light sensing tissue and mediates both image forming vision and non-image forming vision. The classical photoreceptors, rods and cones, are involved in image forming vision. These photoreceptors convert light into an electrical signal that is processed in the retina and ultimately transmitted to the brain via retinal ganglion cells. The phototransduction cascade in rods and cones has been extensively studied and is well understood [28]. In the last decade a small subset of retinal ganglion cells (ipRGCs) have also been shown to be light sensitive photoreceptors (see for reviews [5, 25, 32]). These ganglion cells express the novel visual pigment melanopsin and mediate non-image forming functions. The ipRGCs

*Department of Veterinary & Comparative Anatomy, Pharmacology, and Physiology, Washington State University
†School of Mathematics and Natural Sciences, Arizona State University
‡Department of Biology, University of Maryland, Baltimore County
§Department of Mathematics, Tulane University
¶Department of Mathematics and Statistics, University of Maryland, Baltimore County
‖Department of Mathematics and Statistics, University of Maryland, Baltimore County
**Department of Biology, University of Maryland, Baltimore County
††Department of Mathematics, University of Arizona
‡‡Department of Integrative Physiology & Neuroscience, Washington State University

project to the supra chiasmic nucleus (SCN), and the olivary pretectal nucleus (OPN) where they regulate photoentrainment of circadian rhythms and pupilary light response respectively [9, 14].

Melanopsin is the atypical vertebrate opsin expressed in ipRGCs. Although melanopsin is expressed in the mammalian retina, it is evolutionarily more closely related to R-opsins that are typically expressed in invertebrate photoreceptors [29]. The details of the phototransduction cascade activated by melanopsin have not been definitively elucidated. However, several studies suggest that melanopsin's G-protein mediated phototransduction cascade is similar to that found in Drosophila photoreceptors [10, 17, 38].

The phototransduction cascade governing the photo-response in both rods and cones has been the focus of extensive mathematical modeling [4, 11, 12, 19, 21, 23, 31, 33], using a variety of approaches. Stochastic models including [12] and [4, 11, 31] introduced hybrid stochastic/deterministic models for the photo-response in rods and cones. There has been very little attention focused on mathematical modeling of the phototransduction in ipRGCs. Our focus is to develop a stochastic model of the hypothesized melanopsin phototransduction cascade. We use the chemical reactions in the hypothesized phototransduction cascade and model them as a continuous-time Markov jump process. The model can be also written in terms of the chemical master equation which governs temporal evolution of the probability density of species numbers. Using Gillespie's Stochastic Simulation Algorithm, the exact trajectory of the sample path for the species numbers is computed. The mean and standard deviations of the number of open channels are compared to those of experimental data, where the mean is computed by averaging 4000 realizations of the trajectories for each time point.

We construct a stochastic model of the hypothesized phototransduction cascade. The cascade consists of two phases. The activation phase begins when melanopsin molecules are activated by light which initiates a chemical cascade that ultimately gates open non-specific cation ion channels in the plasma cell membrane. The opening of these channels generates a depolarization in the membrane potential and these electrical signals are then sent to the brain via the optic nerve. The deactivation phase is the biochemical process that returns the activated melanopsin and the light-activated biochemical cascade to its original inactive state. We model 52 chemical reactions in the cascade, involving 33 distinct species. In addition to constructing the chemical pathway, we also identify the initial conditions for all the species and 21 rate constants involved in these reactions. We assume that in this pathway 5 species are abundant and as such we take them to be constant. We determine the parameters, constants, and initial conditions using experimental data from single flash experiments under two different environments. The first set of experimental data that we use to parameterize our model is current recordings from voltage clamped ipRGC

cells. The second set of experimental data is calcium imaging data from melanopsin expressed in human embryonic kidney (HEK) cells. In this environment, a calcium sensitive dye is used and fluorescence is measured then normalized with the maximum value. To illustrate these two environmental conditions in our mathematical model, we fit the rate constants and initial conditions to match the experimental data.

One advantage of transfecting melanopsin into HEK cells is that the HEK cells are more amenable to experimental manipulation. In particular, Cameron and Robinson [3] created two HEK cell lines where either β-arrestin 1 or β-arrestin 2 are overexpressed. The proteins β-arrestin 1 and β-arrestin 2 are important in the deactivation of G-protein coupled receptors. When calcium imaging experiments were repeated using HEK cell lines with overexpressed β-arrestin, data showed a notable increase in the speed of deactivation of the phototransduction cascade. Using the same rate constants as we found to fit the wild type HEK cells, only varying two initial conditions, our model almost exactly fit the experimental data for the overexpressed β-arrestin cell line. In fact, for the calcium imaging data, not only was the stochastic model able to fit the mean of both the wild type data and the overexpressed β-arrestin data, but the stochastic model was also able to reproduce the experimental standard deviations by scaling the rate constants and initial conditions appropriately.

Unlike the rhodopsin phototransduction cascade where the rate constants of the chemical reactions have been measured *in vivo*, there are no measurements of rate constants for the melanopsin phototransduction cascade. In fact, experiments are still on-going to confirm the species involved in the cascade. Thus, part of the challenge of constructing the model was to find reasonable parameters, rate constants, and initial conditions. We fit the parameters, rate constants, and initial conditions to the experimental data manually, by carefully changing one rate constant at a time, until the simulations qualitatively matched the experimental data. Essentially, the set of parameters, rate constants, and initial conditions that best fit the experimental data correspond to an approximate minimizer of the absolute value of the difference of the experimental data and the simulation data. However, there is no reason to expect that there is a unique global minimum. To determine the sensitivity of the parameters to perturbation, we computed the partial rank correlation coefficient using the Latin Hypercube sampling method. Of the 21 rate constants, 7 in HEK environment (or 14 in ipRGC) had significant p-values, and only 6 showed a strong correlation to number of open channels: the same rate constants showed the same degree of correlation for both set of experimental conditions.

Section 2 contains a description of the hypothesized melanopsin phototransduction cascade in terms of a sequence of chemical reactions. Section 3 contains the parameters that represent the best fit results to both the calcium imaging data and the ipRGC data, as well as graphs showing both the experimental data and the simulated curve. The parameters from the

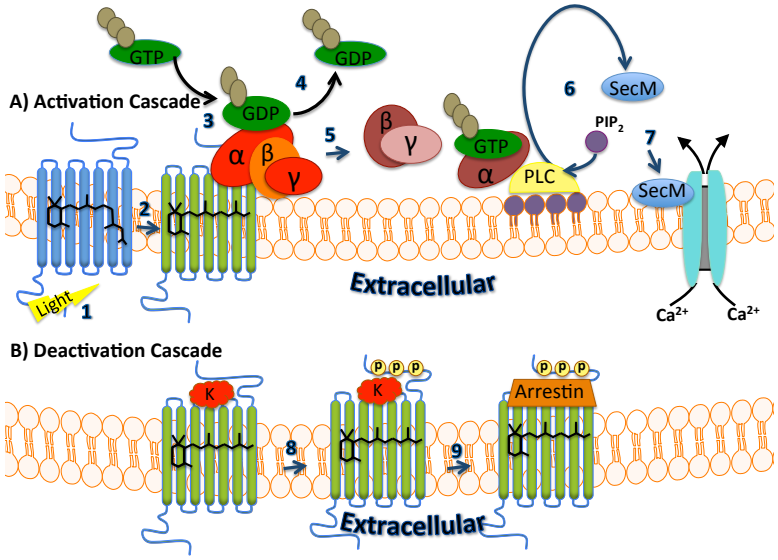

FIG. 1. *Figure 1A illustrates the activation phase of the melanopsin phototransduction cascade. Initiated by a flash of light illustrated by the lightening bolt next to the number 1, light isomerizes 11-cis retinal to the all-trans configuration illustrated by the second step in the figure. In the third step the G-protein binds to the activated melanopsin, and the fourth step exchanges GTP for GDP on the α subunit of the cognite G-protein. The β and γ subunits of the G-protein disassociate from the α subunit of the G-protein, which activates PLC. PLC cleaves PIP_2, creating a second messenger (step 6), which in turn opens the channels. The deactivation phase of the melanopsin phototransduction cascade is illustrated in Figure 1B. A kinase binds to activated melanopsin and phosphorylates the carboxy tail; step 8 in the figure. Our model allows for up to three phosphorylations. Once the tail has been phosphorylated, arrestin binds, which completes the deactivation phase. PLC deactivation described by reactions* (2.10)-(2.12) *are not shown.*

calcium imaging data are fixed and initial conditions adjusted to match experimental results involving overexpressed β-arrestin. Finally, section 4 contains a parameter sensitivity analysis using the Latin hypercube sampling algorithm. The results are discussed in section 5.

2. The Phototransduction Cascade. The melanopsin phototransduction cascade consists of an activation phase and an deactivation phase (see Figure 1). Figure 1A illustrates the activation phase and the deactivation phase is depicted in Figure 1B. The vertebrate phototransduction cascade of melanopsin is hypothesized to be similar to the *Drosophila* photoransduction cascade. We detail the hypothesized pathway below, and indicate which components of this pathway have been experimentally verified.

2.1. Activation. We begin with the activation portion of the cascade, illustrated by steps 1-7 in Figure 1A. Melanopsin's phototransduction cascade is initiated by a single flash response, illustrated by the lightening bolt and step 1 in Figure 1A. Let M_0 denote inactivated, unphosphorylated melanopsin. Activated melanopsin will be denoted by M_n^*, where the subscript n indicates the number of times the carboxy tail has been phosphorylated. We assume that a light flash instantaneously activates some melanopsin molecules, which isomerizes the 11-*cis* retinal to the all-*trans* configuration, illustrated by step 2 in Figure 1. We also assume that previous to the light flash all the melanopsin is inactivated and unphosphorylated:

$$\mathrm{M_0} \xrightarrow{k_L} \mathrm{M_0}^* \tag{2.1}$$

Since this reaction happens once at the beginning of the experiment and the reaction occurs instantaneously, we choose some nonzero initial condition for the amount of activated Melanopsin (M_0^*) and start the simulation immediately after the flash. The activated melanopsin then binds to a G-protein:

$$\mathrm{M_n}^* + \mathrm{G} \cdot \mathrm{GDP} \underset{k_{G2}}{\overset{k_{G1}y(n)}{\rightleftharpoons}} \mathrm{M_n}^* \cdot \mathrm{G} \cdot \mathrm{GDP}, \tag{2.2}$$

as seen in step 3 of Figure 1. Here GDP is guanosine-5'-diphosphate and the function $y(n)$, defined in Table 1, indicates the dependence of the rate constant on the number of phosphorylated sites. The specific G-protein is unknown, however, it is believed to be in the G_q family of G-proteins [10, 17, 38]. The reactions corresponding to step 4 exchange GTP (guanosine-5'-triphosphate) for GDP :

$$\mathrm{M_n}^* \cdot \mathrm{G} \cdot \mathrm{GDP} \xrightarrow{k_{G3}} \mathrm{M_n}^* \cdot \mathrm{G} + \mathrm{GDP} \tag{2.3}$$

$$\mathrm{M_n}^* \cdot \mathrm{G} + \mathrm{GTP} \xrightarrow{k_{G4}} \mathrm{M_n}^* \cdot \mathrm{G} \cdot \mathrm{GTP}. \tag{2.4}$$

Next, the β and γ subunits of the G-protein disassociate (step 5):

$$\mathrm{M_n}^* \cdot \mathrm{G} \cdot \mathrm{GTP} \xrightarrow{k_{G5}} \mathrm{M_n}^* + \mathrm{G}_\alpha \cdot \mathrm{GTP} + \mathrm{G}_{\beta\gamma}. \tag{2.5}$$

The α-subunit then binds to phospholipase-C (PLC):

$$\mathrm{PLC} + \mathrm{G}_\alpha \cdot \mathrm{GTP} \xrightarrow{k_P} \mathrm{PLC}^* \cdot \mathrm{G}_\alpha \cdot \mathrm{GTP}, \tag{2.6}$$

forming the PLC G-protein complex and activating PLC. The activated complex $PLC^* \cdot G_\alpha \cdot GTP$ hydrolyzes phosphatidylinositol 4,5-biphosphate (PIP_2):

$$\mathrm{PIP_2} + \mathrm{PLC}^* \cdot \mathrm{G}_\alpha \cdot \mathrm{GTP} \xrightarrow{k_S} \mathrm{SecM} + \mathrm{PLC}^* \cdot \mathrm{G}_\alpha \cdot \mathrm{GTP}, \tag{2.7}$$

creating second messenger $SecM$, which in turn opens the light-dependent channels:

$$\mathrm{SecM} + \mathrm{Channel}^{\neq} \underset{k_C}{\overset{k_O}{\rightleftharpoons}} \mathrm{SecM} \cdot \mathrm{Channel}^{=}. \tag{2.8}$$

Here, the activated open channel is considered as a complex of transient receptor potential channel C6 and C7 [36, 38].

2.2. Deactivation. Next we describe the deactivation portion of the cascade, illustrated by steps 7-8 in Figure 1B. First, we discuss disassociation of the second messenger $SecM$ from the channel, and the degradation of $SecM$. Channels close as second messenger disassociates, and $SecM$ degrades according to Michaelis-Menten kinetics [30], with rate

$$\delta(SecM) = k_{max} \frac{SecM}{(SecM + K_M)}, \tag{2.9}$$

where K_M is $SecM$ at which δ is half of k_{max}. This model includes the dependence of the degradation of $SecM$ on the number of molecules of $SecM$. Also part of the deactivation is the PLC and G-protein deactivation (not shown in Figure 1). The $PLC^* \cdot G_\alpha \cdot GTP$ complex involves not only the deactivation of PLC, but also the reassociation of the β-γ subunits of the G-protein:

$$\mathrm{PLC}^* \cdot \mathrm{G}_\alpha \cdot \mathrm{GTP} \xrightarrow{k_{I1}} \mathrm{PLC} \cdot \mathrm{G}_\alpha \cdot \mathrm{GDP} \tag{2.10}$$

$$\mathrm{PLC} \cdot \mathrm{G}_\alpha \cdot \mathrm{GDP} \xrightarrow{k_{I2}} \mathrm{PLC} + \mathrm{G}_\alpha \cdot \mathrm{GDP} \tag{2.11}$$

$$\mathrm{G}_\alpha \cdot \mathrm{GDP} + \mathrm{G}_{\beta\gamma} \xrightarrow{k_{I3}} \mathrm{G} \cdot \mathrm{GDP}. \tag{2.12}$$

Deactivation of the melanopsin involves phosphorylation of the carboxy tail, as well as binding of β-arrestin. First a kinase binds to the melanopsin, forming a melanopsin kinase complex:

$$\mathrm{M_n}^* + \mathrm{K} \underset{k_{K2}}{\overset{k_{K1} z(n)}{\rightleftharpoons}} \mathrm{M_n}^* \cdot \mathrm{K}, \tag{2.13}$$

where the function $z(n)$, defined in Table 1, indicates the dependence of the rate constant on the number of phosphorylated sites. Then the tail is phosphorylated by a kinase using adenosine triphosphate (ATP):

$$\mathrm{M_n}^* \cdot \mathrm{K} + \mathrm{ATP} \xrightarrow{k_{K3}} \mathrm{M_{n+1}}^* \cdot \mathrm{K} + \mathrm{ADP}, \tag{2.14}$$

transforming the ATP to ADP (adenosine diphosphate). In this step, the activated melanopsin increases the subscript n to $n+1$ indicating an additional phosphorylation to the carboxy tail. Blasic et al [2] showed that there are six phosphorylation sites on the carboxy tail implicated in phototransduction cascade deactivation. Our model includes three phosphorylation

sites for simplicity. Once the carboxy tail has been phosphorylated, arrestin can bind, quenching the cascade. There are two different isoforms of arrestin expressed in ipRGCs: β-arrestin 1 and β-arrestin 2. Our models allows for either to bind to the tail via the following chemical reactions:

$$\mathrm{M_n}^* + \mathrm{Arr}_{\beta 1} \xrightarrow{k_{B1}w(n)} \mathrm{M_n} \cdot \mathrm{Arr}_{\beta 1} \tag{2.15}$$

$$\mathrm{M_n}^* + \mathrm{Arr}_{\beta 2} \xrightarrow{k_{B2}w(n)} \mathrm{M_n} \cdot \mathrm{Arr}_{\beta 2}, \tag{2.16}$$

where the function $w(n)$ indicates the dependence of the rate constants on the number of phosphorylated sites. We further model the unbinding of the arrestin molecule, and the phosphorylated melanopsin returns to its unactivated state. Once arrestin molecule unbinds from the phosphorylated melanopsin, we consider this melanopsin to be all in the same class and denote this species by M_p. The subscript p indicates that it is phosphorylated (irrespective of the phosphorylation sites).

$$\mathrm{M_n} \cdot \mathrm{Arr}_{\beta 1} \xrightarrow{k_{UB1}w(n)} \mathrm{M_p} + \mathrm{Arr}_{\beta 1} \tag{2.17}$$

$$\mathrm{M_n} \cdot \mathrm{Arr}_{\beta 2} \xrightarrow{k_{UB2}w(n)} \mathrm{M_p} + \mathrm{Arr}_{\beta 2} \tag{2.18}$$

$$\mathrm{M_p} \xrightarrow{k_{De}} \mathrm{M_0} \tag{2.19}$$

Our hypothesized melanopsin phototransduction cascade involves 33 species and 52 reactions. Since the size of the cascade is large, species molecules numbers may have different scales. If the number of molecules of all species is large, the cascade can be modeled using differential equations governing species concentration due to 'law of large numbers' [22]. However, if there is a subset of species whose number of molecules is small, fluctuations of small number of molecules may be important and a stochastic model is needed. Due to the fluctuations in the unscaled experimental data, we model melanopsin phototransduction cascade as a continuous-time Markov jump process which describes evolution of species numbers in time.

A Markov-chain model is also expressed in terms of the chemical master equation which governs evolution of probability density for species numbers. In general, the solution of the chemical master equation cannot be obtained explicitly especially when the cascade involves nonlinear reactions. Instead of solving the equation, stochastic simulation can produce one realization of the sample path of the Markov-chain model. For stochastic simulation of the Markov-chain model for melanopsin phototransduction, we use Gillespie's Stochastic Simulation Algorithm (SSA) [7, 8]. SSA gives one realization of an exact temporal trajectory for the number of molecules of each species. We perform 4000 realizations of simulation and obtain the mean value of the number of open channels by averaging at each time point. We compare these mean values to experimentally measured channel voltage in ipRGC cells and internal calcium levels in HEK cells, with

appropriate scaling. We also compute and scale standard deviations of the species molecules numbers from the data obtained in stochastic simulation and compare them to those of Ca^{2+} expression level in the experimental data. Therefore, the mean of our stochastic model not only fits the average level of experimental data but also fits their fluctuation level, as measured by the standard deviation in both experimental and simulation data.

3. Results. We tested our model using two different types of experiments. First, electrophysiological data collected from ipRGCs in response to a single flash of light illustrates the fast activation and slower deactivation kinetics in the natural environment of melanopsin. Second, we mimic the experimental conditions of calcium imaging experiments in human embryonic kidney (HEK) cells that have been transfected with mouse melanopsin. One advantage of the experiments using transfected tissue culture cells as a model is that is easier to experimentally manipulate conditions. For instance Cameron and Robinson [3] have shown that increased expression of β-arrestin 1 and β-arrestin 2 in the HEK cell environment increases the speed of deactivation. In this section, we show numerical simulations that correspond to the natural environment of ipRGCs as well as the wild type calcium imaging data. We further demonstrate that the overexpressed β-arrestin in the HEK cell environment can be achieved using the stochastic model by only changing the initial conditions and the scaling constant.

3.1. Model Parameters. The rate constants, initial conditions, and constants were fit to wild type data for both the ipRGC cells and the HEK cells expressing melanopsin. There are several model assumptions that were made in fitting the data. First, we assumed that the rates of G protein, kinase and β-arrestin binding depend on the number of sites phosphorylated. This assumption is based on data from an analogous situation with rhodopsin, the visual pigment expressed in rod photoreceptors [18, 20, 27, 35]. To this end, we define three functions y, z, and w to model this dependence on number of phosphorylations in Table 1. The functions y and z are decreasing functions of n, the number of phosphorylations of the carboxy tail, indicating that as the number of phosphorylations increases, the less likely it is for the G-protein and kinase to bind to it. The function w is an increasing function of n, meaning that as the number of phosphorylations of the carboxy tail increases the more likely it is for arrestin to bind and inactivate the melanopsin. The functional forms of y, x, w were chosen to have features which are consistent with the known biological information, but there is no experimental data that supports these specific functional forms. The rate constants were fit to the wild type experimental data using initial conditions inspired by a related deterministic model, and hand tuned to improve the fit. The rate constants that were used to qualitatively fit the wild type data for both the HEK cells and the ipRGCs are shown in Table 2. Rate constants that differ by more than an order of

Function	Reaction Modified
$y(n) = e^{-n/1000}$	modifies G protein binding rates in reaction (2.2)
$z(n) = e^{-2n}$	modifies kinase binding rates in reaction (2.13)
$w(n) = 1 - e^{-100n}$	modifies rates of arrestin binding/unbinding in reactions (2.15), (2.16), (2.17), (2.18)

TABLE 1

Functions y, z, and w are used to modify the rate constants as a function of the number of phosphorylations of the carboxy tail.

magnitude are shaded in gray. A comparison of the rate constants in both environments can be found in Section 5.

Next, we assume that the numbers of molecules of GTP, PIP_2, K, and ATP do not vary significantly during the simulation due to their large quantity, therefore we can choose them as constant. These constants can be embedded in the corresponding reaction rate constants, and we thus treat each of $k_{G4} \cdot GTP$, $k_S \cdot PIP_2$, $k_{K1} \cdot K$, and $k_{K3} \cdot ATP$ as one reaction rate constant. We further assume that the total number of channels is constant as well. We chose there to be 550 channels in both environments with wild type of melanopsin [15], and initially we assume that they are all closed. Finally, we have to initialize the number of molecules for each variable. The non-zero initial conditions are displayed in Table 3.

3.1.1. Results for ipRGCs. IpRGC data was collected from whole-cell currents from a mouse ipRGC in a retinal flat (or whole) mount preparation using a patch clamp recording technique. The cells were held at -60 mV in the presence of synaptic blockers and tetrodotoxin (TTX), a neurotoxin that blocks action potentials by blocking voltage-gated sodium channels. Light responses were elicited by 25 ms pulses of 480 nm light with a maximum intensity of 3×10^{13} photons $cm^{-2}\, s^{-1}$. Experimental results are shown by the light gray line in Figure 2. The electrophysiological data is from a voltage clamp cell, so the inward current in Figure 2 represents the depolarization that is observed *in vivo*. The current values are normalized so that the maximum value of the centerline in time becomes 1. Then, they are reflected across the horizontal axis to compare them to simulation data. We assume that the fluctuations in the experimental data are due to inherent noise in the system as well as fluctuations from the recording apparatus. Thus, we focus on matching the mean of the data, and do not try to capture the fluctuations with our model.

The phototransduction cascade was simulated using the Gillespie's SSA with the rate constants, parameters, and initial conditions listed in the tables in Section 3.1. The results of the simulation averaged over 4000 realizations of the simulation are plotted with the experimental data in Figure 2. The averaged simulation is represented by the solid black curve in the figure, and the experimental data is given by the gray-scale recording

Params	Rates	HEK cells	ipRGCs
$k_{G1}\ y(n)$	G protein binding for M_n^*	10.9091 $y(n)$	18.1818 $y(n)$
k_{G2}	G protein unbinding	0.8	2
k_{G3}	GDP unbinding from G protein	0.9	50
$k_{G4} \cdot GTP$	GTP binding	1.0886	50
k_{G5}	disassociation of subunits	3.5	50
k_P	G protein binding to PLC	0.9091	9.0909
k_{I1}	PLC deactivation	15	150
k_{I2}	PLC disassociation	0.673	7
k_{I3}	Reassociation of subunits	0.0018	0.0036
$k_S \cdot PIP_2$	(SecM) production	11.5	60
k_{max}	maximum SecM degradation	6.05	38.5
K_M	half-life of SecM degradation	6.05	1.1
k_{O}	channel opening	0.0036	0.7273
k_{C}	channel closing	0.06	35
$k_{K1} \cdot K \times z(n)$	kinase binding for M_n^*	8 $z(n)$	15 $z(n)$
k_{K2}	kinase unbinding	8	15
$k_{K3} \cdot ATP$	phosphorylation	10	15
$k_{B1}\ w(n)$	β-arrestin 1 binding for M_n^*	2.7273 $w(n)$	90.9091 $w(n)$
$k_{B2}\ w(n)$	β-arrestin 2 binding for M_n^*	2.7273 $w(n)$	90.9091 $w(n)$
$k_{UB1}\ w(n)$	β-arrestin 1 unbinding for M_n^*	0.1 $w(n)$	0.01 $w(n)$
$k_{UB2}\ w(n)$	β-arrestin 2 unbinding for M_n^*	0.1 $w(n)$	0.01 $w(n)$
k_{De}	melanopsin deactivation	0.2	20

TABLE 2

The rate constants for the melanopsin phototransduction cascade for both the HEK cell environment and the ipRGC environment are displayed above. The rate constants whose differences between HEK cell environment and the ipRGC environment are different by more than an order of magnitude are shaded in gray. The functions y, z, and w are defined in Table 1.

for a timescale of approximately 5 seconds. The simulation captures the deactivation part of the phototransduction cascade well. The activation part of the simulation is not quite as fast as the experimental data, but still gives a reasonable representation of the data. The exceptional fit that we get from simulation of the 52 reactions with 33 variables validates that our model qualitatively captures the mean trend in the experimental data.

Variables	Non-zero Initial Conditions	HEK cells	ipRGCs
$M_0^*(0)$	number of M_0^* molecules	86	86
$G \cdot GDP(0)$	number of molecules of $G \cdot GDP$	33	33
$PLC(0)$	number of PLC molecules	13	13
$Channel^{\neq}(0)$	number of closed channels	550	550
$Arr\beta_1(0)$	number of molecules of β-arrestin 1	22	22
$Arr\beta_2(0)$	number of molecules of β-arrestin 2	22	22

TABLE 3
The nonzero initial conditions used in the simulation are listed in this table.

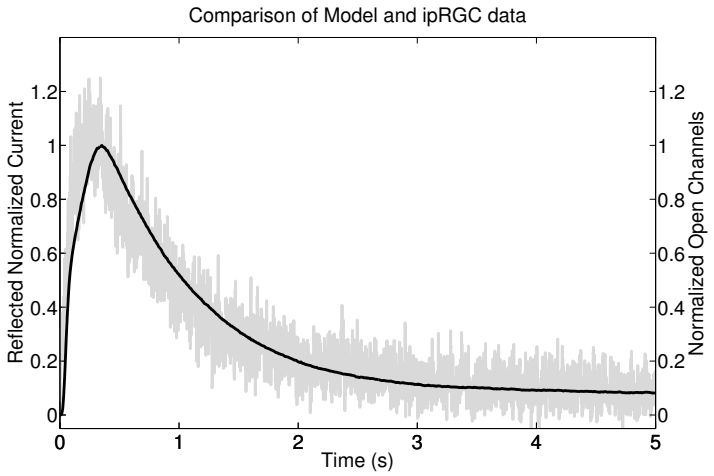

FIG. 2. *Fraction of open channels from the simulated model (black curve) are plotted as a function of time on the same graph as the experimental data (gray-scale recordings) shown as reflected normalized current.*

3.1.2. Results for Calcium Imaging Data. Data from calcium imaging experiments was collected using HEK cells. HEK-293 cells were transfected with wild type mouse melanopsin (opn4m, accession NP_038915). Cells were plated with 50000 cells in each of 8 wells of a 96 well plate. Cells were loaded with a calcium indicator dye ($4\,\mu M$ Fluo-4 AM (Invitrogen)). Melanopsin was regenerated with $20\,\mu M$ 11-*cis* retinal. Cells were exposed to a flash of light of wavelength $488\,nm$ once per second for 60 seconds, and the fluorescence was measured ((wavelength $525\,nm$) once per second for 60 seconds) using a Tecan Infinite 200 microplate reader (Tecan Group Ltd.). The baseline fluorescence was subtracted. The responses of all successfully transfected cells were averaged, and both the

mean and standard deviations of the responses were normalized by the maximum mean value so that it can be compared with the mathematical model.

The wild type experimental data is shown by the gray curve in Figure 3. The gray error bars represent one standard deviation from the mean of the experimental data. Similarly, the averaged simulation of the phototransduction cascade in HEK cells over 4000 realizations using Gillespie's SSA is shown with the black line in Figure 3. Black dotted lines represent one standard deviations from the mean of the simulated data in the figure. We compute mean and standard deviations of the number of open channels and scale those by the maximum value of the mean open channel in time so that simulation result can be compared with the scaled experimental data. The simulation of the phototransduction cascade in HEK cells fits the experimental data almost exactly. When we fit the stochastic simulation result to the experimental data, we fit both the scaled mean and the standard deviations of the open channels. We first fit the scaled mean value. Since the scaled mean value is the ratio between the mean number of open channels and its maximum value, this value does not change if we change the number of molecules in the system keeping the ratio between molecule numbers of species. Therefore, using standard techniques in stochastic simulation, we change the system volume to fit the standard deviations of the simulation to those of experimental data. When we change the system volume, the number of molecules and reaction rate constants whose reactions are not first order are changed. For more details about the relationship between stochastic reaction rate constants and the system volume, see [22].

Calcium imaging data was also obtained from HEK293 cells lines that were generated to overexpress either β-arrestin 1 or 2. Light activation of melanopsin was measured using the calcium indicator assay as described for the wild type cell line. Figure 4 shows fitting between overexpressed β-arrestin experimental data and our simulation results. As in Figure 3, the gray curve and gray error bar represent the scaled values of the mean and standard deviations from the mean of the experimental data. The black line and the black dotted lines are the scaled mean and standard deviations from the mean of the number of open channels. To reproduce experimental data with overexpression of β-arrestin using the stochastic model, we use the same set of the parameters used in the wild type simulation except for the the initial number of open channels and the initial number of molecules of β-arrestin 1 or 2. Since fluctuations in overexpressed β-arrestin experimental data are different from those in the wild type data, we use a scaling constant (0.8182 for β-arrestin 1 and 7.2727 for β-arrrestin 2) to increase or decrease fluctuation levels. A scaling constant is multiplied to all initial conditions, k_{max}, and K_M. All second-order reaction constants with both reactants varying in time (k_{B1}, k_{B2}, k_O, k_{I3}, k_P, and k_{G1}) were divided by the scaling constant. With the modification using the scaling constant, we

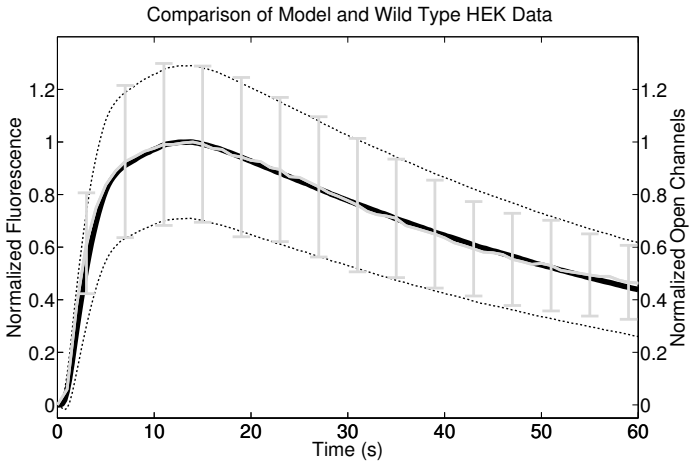

FIG. 3. *Experimental data from calcium imaging experiments are plotted as a function of time. Gray solid line and error bars are the mean and the standard deviations from the mean in the experimental results represented as normalized fluorescence. On the same figure, black solid line and dotted lines are the normalized mean and standard deviations from the mean of the number of open channels in the stochastic simulation.*

can keep the same value for scaled mean number of open channels and reduce the scaled standard deviations. Fitting between experimental data and simulation are exact with slight difference around the peaks. The fact that we can fit the scaled mean value of the overexpressed β-arrestin data by slightly modifying initial conditions of two species and incorporating the same set of parameters values used in the wild type simulation before scaling validates our model and its hypotheses.

4. Parameter sensitivity analysis. In order to perform sensitivity analysis of the model parameters, we employed a method of partial rank correlation coefficient (PRCC) using techniques from [26] for stochastic simulation. Each parameter was allowed to vary from half of the estimated value to twice of the estimated value. Using Latin Hypercube sampling method, each parameter was sampled from a uniformly distributed interval. A single stochastic simulation was run using the sampled parameters, and the resulting number of open channels at the ending time, 5 seconds for ipRGC and 60 seconds for HEK cells, was calculated. We repeated this process for 4000 realizations and each realization was computed with a set of newly sampled parameters. Sampled parameters and the number of open channels are transformed into rank values and we computed PRCCs of the parameters. PRCCs in two environments, ipRGC and HEK, are given in Figure 4. Our null hypothesis is that PRCC between the parameter and the number of open channels is not significantly different from zero. If p-value of each parameter is less than 0.01, we strongly reject the null hy-

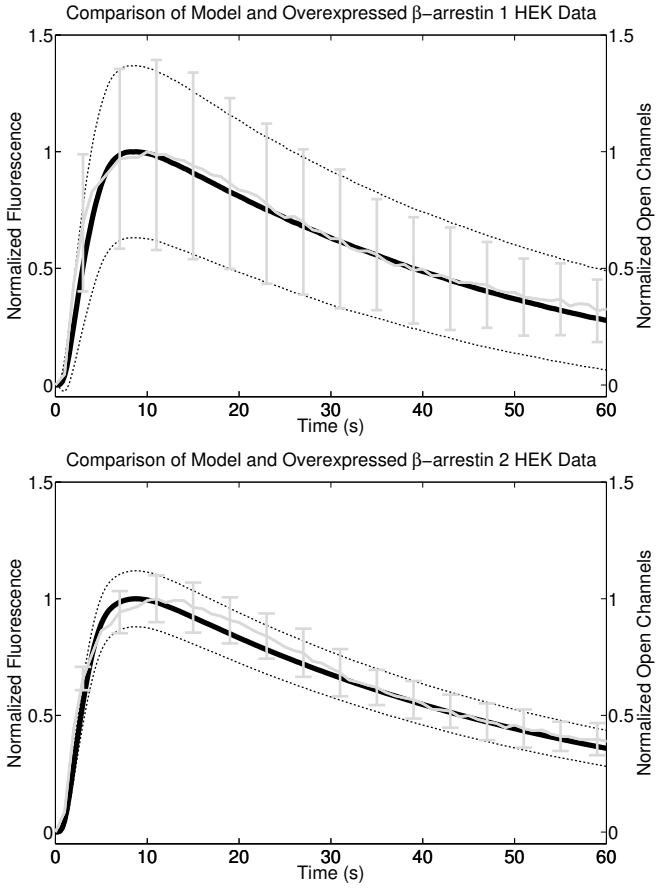

FIG. 4. *Experiments in HEK cells with increased values of β-arrestin 1 and β-arrestin 2 over the wild type showed an increased speed of deactivation. Experimental results with error bars representing the standard deviation are plotted along with simulated values. Parameters are exactly as the wild type calcium imaging except for scaling, but with different initial conditions to simulate the increased values of β-arrestin 1 and β-arrestin 2, respectively. In the top panel, the initial number of open channels and that of molecules of β-arrestin 1 are set as* 275 *and* 33*. In the bottom panel, the initial number of open channels and that of molecules of β-arrestin 2 are set as* 385 *and* 33*. In both cases, other initial conditions are set to be the same as the wild type simulation. Then, all initial conditions and some rate constants are scaled by* 0.8182 *(top) and* 7.2727 *(bottom) to match standard deviations of simulation and experimental data.*

pothesis, which means that PRCC between the parameter and the number of open channels is significantly different from zero. Therefore, we are only interested in the statistically significant case with p-value less than 0.01. In Table 4, parameters with p-value less than 0.01 in the ipRGC environment are given with their PRCCs and ranges of the sampled parameters. Simi-

larly in Table 5, parameters in the HEK environment with p-value less than 0.01 are listed. The parameters with p-values close to zero are statistically highly significant.

PRCC is a correlation coefficient, so it is between ± 1. The closer the PRCC is to ± 1, the ranks of the number of open channels and the corresponding parameter have strong linear correlation. If the PRCC is close to 0, the rank of the number of open channels has no or weak correlation with the rank of the corresponding parameter. In general, model parameters are more sensitive under the HEK environment than under ipRGC environment comparing the ranges of PRCC in Figures 4 and 5. Interestingly, statistically significant parameters with a certain amount of correlation with the number of open channels are similar under two environment: k_{max}, K_M, k_{I1}, k_{I3}, $k_S \cdot PIP_2$, k_O, and k_C. In the ipRGC environment, K_M, k_{I3}, $k_S \cdot PIP_2$, and k_O are slightly positively correlated and k_{max}, k_{I1}, and k_C are slightly negatively correlated with the number of open channels. In the HEK environment, K_M, $k_S \cdot PIP_2$, and k_O are strongly positively correlated and k_{max}, k_{I1}, and k_C are strongly negatively correlated with the number of open channels. The rate constant k_{I3} is slightly positively correlated and k_{UB2} is slightly negatively correlated with the number of open channels.

Surprisingly, the rate constants associated with the G-protein cascade k_{G1-5} and the rate constant associated with PLC binding k_P either were not sensitive or had only a slight correlation in either environment. The rate constants associated with the unbinding of β-arrestin k_{UB1} and k_{UB2} either were not sensitive or had only a slight negative correlation on the number of open channels in both environments. The parameters with the strongest correlation, positive or negative, were associated with either the production ($k_S \cdot PIP_2$), degradation (k_{max}, K_M), or binding or unbinding (k_O, k_C) of SecM to the channels. The rate constants associated with deactivation of PLC k_{I1} and k_{I3} had a strong negative correlation and a significant level of positive correlation, respectively, on the number of open channels in both environments. The HEK cell environment seemed more sensitive to the changes in these parameters than the ipRGC environment based on the magnitude of the PRCC.

5. Discussion. Based on the hypothesized phototransduction pathway of melanopsin, a stochastic model was developed that qualitatively reproduced experimental data from two different experimental paradigms. First, we were able to produce a set of parameters, rate constants, and initial conditions for the stochastic model so that the mean of 4000 realizations of the phototransduction cascade corresponded to experimental data collected using voltage clamp from ipRGCs. We were also able to find a set of parameters, rate constants and initial conditions for the stochastic model so that the mean and standard deviation of 4000 realizations of the hypothesized phototransduction cascade matched mean and standard deviation of

Params	Ranges	PRCC in ipRGC	p-value in ipRGC
k_{max}	$[19.25, 77]$	-0.3151	6.4813×10^{-93}
K_M	$[0.55, 2.2]$	0.1687	6.4901×10^{-27}
k_{I1}	$[75, 300]$	-0.2830	1.4916×10^{-74}
k_{I3}	$[0.0018, 0.0073]$	0.2579	8.7588×10^{-62}
$k_S \cdot PIP_2$	$[30, 120]$	0.2792	1.5149×10^{-72}
k_O	$[0.3636, 1.4545]$	0.2671	2.6029×10^{-66}
k_C	$[17.5, 70]$	-0.3010	1.5309×10^{-84}

TABLE 4
PRCCs and p-values in ipRGC

Params	Ranges	PRCC in HEK cells	p-value in HEK cells
k_{G2}	$[0.4, 1.6]$	-0.0472	0.0028
$k_{G4} \cdot GTP$	$[0.5443, 2.1772]$	-0.0775	9.3255×10^{-7}
k_{max}	$[3.0250, 12.1]$	-0.5451	1.7026×10^{-308}
K_M	$[3.0250, 12.1]$	0.4897	2.5927×10^{-240}
k_{I1}	$[7.5, 30]$	-0.5997	0
k_{I2}	$[0.3365, 1.3460]$	0.0655	3.4113×10^{-5}
k_{I3}	$[0.0009, 0.0036]$	0.1481	4.6334×10^{-21}
$k_S \cdot PIP_2$	$[5.75, 23]$	0.5986	0
k_O	$[0.0018, 0.0073]$	0.5222	8.2804×10^{-279}
k_C	$[0.03, 0.12]$	-0.5402	6.8776×10^{-302}
$k_{K1} \cdot K$	$[4, 16]$	-0.0615	9.9019×10^{-5}
$k_{K3} \cdot ATP$	$[5, 20]$	-0.0476	0.0026
k_{UB1}	$[0.05, 0.2]$	-0.0662	2.8055×10^{-5}
k_{UB2}	$[0.05, 0.2]$	-0.1143	4.2536×10^{-13}

TABLE 5
PRCCs and p-values in HEK cells

the wild type data from calcium imaging experiments in HEK cells transfected with mouse melanopsin. We were also able to match the mean and standard deviation of the calcium imaging experiments on HEK cell lines that overexpressed β-arrestin by only changing two initial conditions in the model, otherwise using the same rate constants and parameters as found for the HEK wild type cell line, and scaling initial conditions, rate constants, and parameters appropriately to match the fluctuation levels. Our simulations provide strong evidence that melanopsin has a robust phototransduction cascade that is similar with that of invertebrate (*Drosophila*) photoreceptors.

Table 2 contains the best fit rate constants for the ipRGC and HEK cells. Melanopsin is naturally expressed in ipRGCs, thus these rate con-

stants more likely correspond to those measured in ipRGCs. However, there is no reason to believe that the rate constants in HEK cells are the same, and in fact, for our simulations, the rate constants highlighted in Table 2 differ by more than an order of magnitude between the ipRGC and HEK cell environments. There are several reasons to expect differential rate constants. First, if ipRGCs are indeed similar to *Drosophila* photoreceptors where many of the key proteins involved in phototransduction are localized in a "signalplex" [24, 34], then the key proteins involved in phototransduction in ipRGCs maybe localized in a similar molecular structure. This hypothesized signalplex could speed up the phototransduction cascade in ipRGCs as compared to the signaling observed in transfected HEK cells. Second, the ionic environment and regulation of calcium maybe different in HEK cells as compared to ipRGCs. Calcium is a key ion involved in the regulation of many cytosolic enzymes. Thirdly, the calcium released and measured in HEK cells is most likely being released from internal stores and the actual channel being opened may differ from the channel in ipRGCs. Finally, the lipids that make up the plasma membrane in ipRGCs and HEK cells could be different. It has been demonstrated that lipids are important in the regulation of TRP channels in *Drosophila* photoreceptors [13].

There are actually five morphological subtypes of melanopsin expressing retinal ganglion cells [1, 32]. The simulations and experimental data shown here correspond to M1 cells. The kinetics of the light response for the subtypes M2-M5 are known to be different than those of the M1 subclass, yet the mechanisms underlying these physiological differences have not yet been elucidated [16]. Our parameter sensitivity analysis suggests that in order to significantly change the time course of the light-activated response of M1 ipRGCs, the rate constants associated with the production, degradation, or binding of $SecM$ have the strongest correlation with the number of open channels and a p-value that makes it statistically significant. Thus our work suggests experiments that altered the rate constants of the enzymes involved in regulating second messenger concentration will alter the kinetics of the light responses of M2-M5.

The focus of both the simulations and experimental data presented here is the biochemical response of dark-adapted cells to a single light flash. Light adaptation is defined as the change in response of a photoreceptor to either a sustained background light or to a series of light flashes. Like most photoreceptors, ipRGCs adapt to background light of various intensities and exhibit adaptation when responding to a series of light flashes [6, 37]. ipRGCs respond to a series of identical light flashes by a decrease in the size of the response and acceleration of the kinetics (results not shown). We used our model to simulate a series of light flashes and our model was able to reproduce the decrease in amplitude but not the increase in the response kinetics. Therefore, our model needs to be modified to incorporate the biochemical mechanisms underlying adaptation in ipRGCs. These mechanisms have yet to be elucidated but may include calcium regula-

tion, and phosphorylation of melanopsin by both Protein Kinase A and a G-protein coupled receptor kinase.

Acknowledgements. The authors gratefully acknowledge the support of the Institute for Mathematics and its Applications (IMA), where this work was initiated. This research has been supported in part by the National Institutes of Health under grant R01EY019053 (P.R.R.) and MH67094 (R.L.B.). E.G.C. was supported by National Institutes of Health under training grant NIH/NIGMS T32GM066706.

REFERENCES

[1] D. M. Berson, A. M. Castrucci, and I. Provencio, *Morphology and mosaics of melanopsin-expressing retinal ganglion cell types in mice*, Journal of Comparative Neurology, 518 (2010), pp. 2405–2422.

[2] J. R. Blasic Jr., V. Matos-Cruz, D. Ujla, E. G. Cameron, S. Hattar, M. E. Halpern, and P. R. Robinson, *Identification of critical phosphorylation sites on the carboxy tail of melanopsin*, Biochemistry, 53 (2014), pp. 2644–2649.

[3] E. G. Cameron and P. R. Robinson, *Beta-arrestin dependent deactivation of mouse melanopsin*. under review, 2014.

[4] G. Caruso, P. Bisegna, D. Andreucci, L. Lenoci, V. V. Gurevich, H. E. Hamm, and E. DiBenedetto, *Identification of key factors that reduce the variability of the single photon response*, Proceedings of the National Academy of Sciences, 108 (2011), pp. 7804–7807.

[5] M. T. H. Do and K.-W. Yau, *Intrinsically photosensitive retinal ganglion cells*, Physiological Reviews, 90 (2010), pp. 1547–1581.

[6] ———, *Adaptation to steady light by intrinsically photosensitive retinal ganglion cells*, Proceedings of the National Academy of Sciences, 110 (2013), pp. 7470–7475.

[7] D. T. Gillespie, *A general method for numerically simulating the stochastic time evolution of coupled chemical reactions*, Journal of Computational Physics, 22 (1976), pp. 403–434.

[8] ———, *Exact stochastic simulation of coupled chemical reactions*, Journal of Physical Chemistry, 81 (1977), pp. 2340–2361.

[9] J. J. Gooley, J. Lu, D. Fischer, and C. B. Saper, *A broad role for melanopsin in nonvisual photoreception*, Journal of Neuroscience, 23 (2003), pp. 7093–7106.

[10] D. M. Graham, K. Y. Wong, P. Shapiro, C. Frederick, K. Pattabiraman, and D. M. Berson, *Melanopsin ganglion cells use a membrane-associated rhabdomeric phototransduction cascade*, Journal of Neurophysiology, 99 (2008), pp. 2522–2532.

[11] R. D. Hamer, S. C. Nicholas, D. Tranchina, T. D. Lamb, and J. L. P. Jarvinen, *Toward a unified model of vertebrate rod phototransduction*, Visual Neuroscience, 22 (2005), pp. 417–436.

[12] R. D. Hamer, S. C. Nicholas, D. Tranchina, P. A. Liebman, and T. D. Lamb, *Multiple steps of phosphorylation of activated rhodopsin can account for the reproducibility of vertebrate rod single-photon responses*, Journal of General Physiology, 122 (2003), pp. 419–444.

[13] R. C. Hardie, *TRP channels and lipids: from Drosophila to mammalian physiology*, Journal of Physiology, 578 (2007), pp. 9–24.

[14] S. Hattar, M. Kumar, A. Park, P. Tong, J. Tung, K.-W. Yau, and D. M. Berson, *Central projections of melanopsin-expressing retinal ganglion cells in the mouse*, Journal of Comparative Neurology, 497 (2006), pp. 326–349.

[15] T. Hofmann, A. G. Obukhov, M. Schaefer, C. Harteneck, T. Gudermann,

and G. Schultz, *Direct activation of human TRPC6 and TRPC3 channels by diacylglycerol*, Nature, 397 (1999), pp. 259–263.

[16] C. Hu, D. J. D. Hill, and K. Y. Wong, *Intrinsic physiological properties of the five types of mouse ganglion-cell photoreceptors*, Journal of Neurophysiology, 109 (2013), pp. 1876–1889.

[17] S. Hughes, A. Jagannath, , D. Hickey, S. Gatti, M. Wood, S. N. Peirson, R. G. Foster, and M. W. Hankins, *Using siRNA to define functional interactions between melanopsin and multiple G protein partners*, Cellular and Molecular Life Sciences, (2014). DOI 10.1007/s00018-014-1664-6.

[18] J. B. Hurley, M. Spencer, and G. A. Niemi, *Rhodopsin phosphorylation and its role in photoreceptor function*, Vision Research, 38 (1998), pp. 1341–1352.

[19] B. M. Invergo, L. Montanucci, K.-W. Koch, J. Bertranpetit, and D. Dell'Orco, *Exploring the rate-limiting steps in visual phototransduction recovery by bottom-up kinetic modeling*, Cell Communication and Signaling, 11 (2013), p. 36.

[20] M. J. Kennedy, F. A. Dunn, and J. B. Hurley, *Visual pigment phosphorylation but not transducin translocation can contribute to light adaptation in zebrafish cones*, Neuron, 41 (2004), pp. 915–928.

[21] J. I. Korenbrot, *Speed, adaptation, and stability of the response to light in cone photoreceptors: The functional role of Ca-dependent modulation of ligand sensitivity in cGMP-gated ion channels*, Journal of General Physiology, 139 (2012), pp. 31–56.

[22] T. G. Kurtz, *The relationship between stochastic and deterministic models for chemical reactions*, Journal of Chemical Physics, 57 (1972), pp. 2976–2978.

[23] T. D. Lamb and E. N. Pugh Jr., *A quantitative account of the activation steps involved in phototransduction in amphibian photoreceptors*, Journal of Physiology, 449 (1992), pp. 719–758.

[24] W. Liu, W. Wen, Z. Wei, J. Yu, F. Ye, C.-H. Liu, R. C. Hardie, and M. Zhang, *The INAD scaffold is a dynamic, redox-regulated modulator of signaling in the Drosophila eye*, Cell, 145 (2011), pp. 1088–1101.

[25] R. J. Lucas, *Mammalian inner retinal photoreception*, Current Biology, 23 (2013). R125-133.

[26] S. Marino, I. B. Hogue, C. J. Ray, and D. E. Kirschner, *A methodology for performing global uncertainty and sensitivity analysis in systems biology*, Journal of Theoretical Biology, 254 (2008), pp. 178–196.

[27] A. Mendez, M. E. Burns, A. Roca, J. Lem, L.-W. Wu, M. I. Simon, D. A. Baylor, and J. Chen, *Rapid and reproducible deactivation of rhodopsin requires multiple phosphorylation sites*, Neuron, 28 (2000), pp. 153–164.

[28] K. Palczewski, *Chemistry and biology of vision*, Journal of Biological Chemistry, 287 (2012), pp. 1612–1619.

[29] M. L. Porter, J. R. Blasic, M. J. Bok, E. G. Cameron, T. Pringle, T. W. Cronin, and P. R. Robinson, *Shedding new light on opsin evolution*, Proceedings of the Royal Society B: Biological Sciences, (2011). rspb.2011.1819.

[30] C. V. Rao and A. P. Arkin, *Stochastic chemical kinetics and the quasi-steady-state assumption: Application to the Gillespie algorithm*, Journal of Chemical Physics, 118 (2003), pp. 4999–5010.

[31] J. Reingruber, J. Pahlberg, M. L. Woodruff, A. P. Sampath, G. L. Fain, and D. Holcman, *Detection of single photons by toad and mouse rods*, Proceedings of the National Academy of Sciences, 110 (2013), pp. 19378–19383.

[32] T. M. Schmidt, M. T. H. Do, D. Dacey, R. Lucas, S. Hattar, and A. Matynia, *Melanopsin-positive intrinsically photosensitive retinal ganglion cells: From form to function*, Journal of Neuroscience, 31 (2011), pp. 16094–16101.

[33] L. Shen, G. Caruso, P. Bisegna, D. Andreucci, V. V. Gurevich, H. E. Hamm, and E. DiBenedetto, *Dynamics of mouse rod phototransduction and its sensitivity to variation of key parameters*, IET Systems Biology, 4 (2010), pp. 12–32.

[34] B.-H. Shieh and M.-Y. Zhu, *Regulation of the TRP Ca^{2+} channel by INAD in Drosophila photoreceptors*, Neuron, 16 (1996), pp. 991–998.

[35] S. A. Vishnivetskiy, D. Raman, J. Wei, M. J. Kennedy, J. B. Hurley, and V. V. Gurevich, *Regulation of arrestin binding by rhodopsin phosphorylation level*, Journal of Biological Chemistry, 282 (2007), pp. 32075–32083.

[36] E. J. Warren, C. N. Allen, R. L. Brown, and D. W. Robinson, *Intrinsic light responses of retinal ganglion cells projecting to the circadian system*, European Journal of Neuroscience, 17 (2003), pp. 1727–1735.

[37] K. Y. Wong, F. A. Dunn, and D. M. Berson, *Photoreceptor adaptation in intrinsically photosensitive retinal ganglion cells*, Neuron, 48 (2005), pp. 1001–1010.

[38] T. Xue, M. T. H. Do, A. Riccio, Z. Jiang, J. Hsieh, H. C. Wang, S. L. Merbs, D. S. Welsbie, T. Yoshioka, P. Weissgerber, S. Stolz, V. Flockerzi, M. Freichel, M. I. Simon, D. E. Clapham, and K.-W. Yau, *Melanopsin signalling in mammalian iris and retina*, Nature, 479 (2011), pp. 67–73.

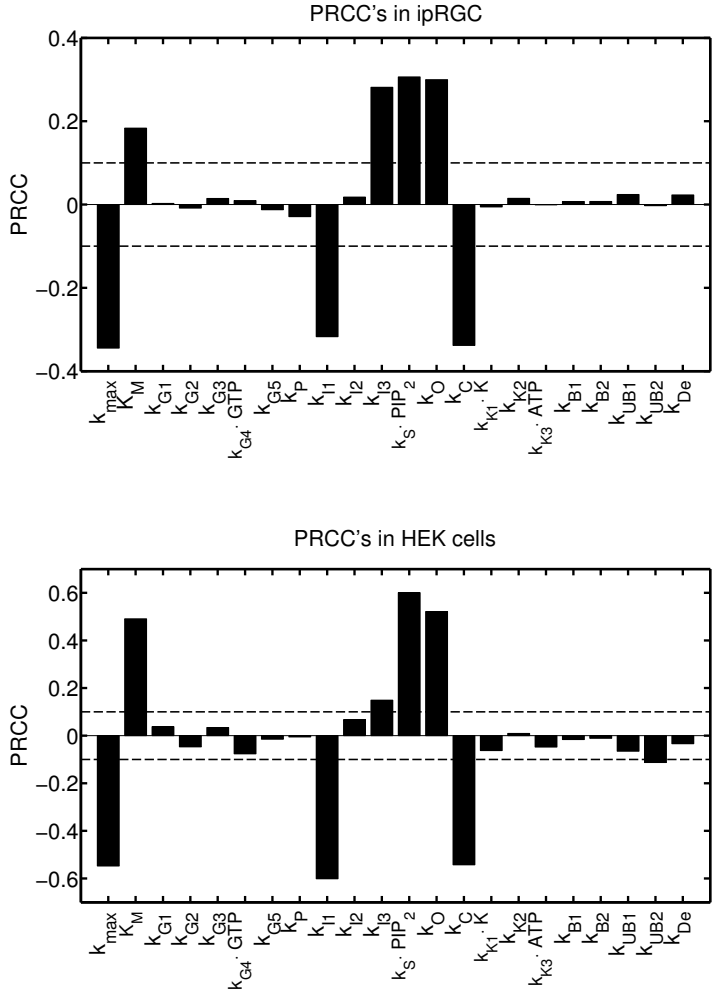

FIG. 5. *A method of partial rank correlation coefficient (PRCC) is used with stochastic simulation. PRCCs of the rate constants with the number of open channels in the ipRGC environment are given on the top and those in the HEK cells are given on the bottom.The dashed lines at* ± 0.1 *represent artificial thresholds to indicate sensitive parameters. The parameters* k_{max}, K_M, k_{I1}, k_{I3}, $k_S \cdot PIP_2$, k_O, *and* k_C *are statistically significant with p-values less than* 0.01 *in both environment. Additionally,* k_{G2}, $k_{G4} \cdot GTP$, k_{I2}, $k_{K1} \cdot K$, $k_{K3} \cdot ATP$, k_{UB1}, *and* k_{UB2} *are statistically significant in the HEK environment.*